Forbidden Decays of Hydrogenlike and Heliumlike Argon*

Richard Marrus and Robert W. Schmieder
Lawrence Radiation Laboratory, Berkeley, California 94720
(Received 11 August 1971)

Four forbidden decay modes of hydrogenlike argon (Ar^{+17}) and heliumlike argon (Ar^{+16}) have been observed and the lifetimes of the states decaying via these modes have been measured by a beam-foil time-of-flight technique. The decays are the two-photon decay $2^2S_{1/2} \rightarrow 1^2S_{1/2}$ of Ar^{+17}, the two-photon decay $2^1S_0 \rightarrow 1^1S_0$ of Ar^{+16}, the relativistically induced magnetic dipole decay $2^3S_1 \rightarrow 1^1S_0$ of Ar^{+16}, and the magnetic quadrupole decay $2^3P_2 \rightarrow 1^1S_0$ of Ar^{+16}. The measured lifetimes of the levels are $\tau(2^2S_{1/2}) = 3.54 \pm 0.25$ nsec, $\tau(2^1S_0) = 2.3 \pm 0.3$ nsec, $\tau(2^3P_2) = 1.7 \pm 0.3$ nsec, and $\tau(2^3S_1) = 172 \pm 30$ nsec. From the agreement between the measured and calculated lifetimes it is possible to place an upper limit on the amount of parity impurity in the $2^2S_{1/2}$-state wave function of hydrogenlike Ar^{+17}. Writing $\psi(2^2S_{1/2}) = \Phi(2^2S_{1/2}) + \epsilon\Phi(2^2P_{1/2})$, where the Φ's are the Schrödinger solutions to the hydrogen atom, we obtain $|\epsilon| \leq 6 \times 10^{-4}$.

INTRODUCTION

In spite of the fact that the hydrogen and helium spectra can probably qualify among the most studied problems in the history of physics, there is relatively little experimental information concerning the forbidden decays, i.e., those decays which proceed by other than an allowed electric dipole transition. These decays were first considered in a classic paper by Breit and Teller,[1] and it is now accepted that the $2^2S_{1/2}$ state of hydrogen and the 2^1S_0 state of helium decay primarily by two-photon emission, while the 2^3S_1 state of helium decays by a relativistically induced magnetic dipole transition. As will be discussed later, it is now clear that, for heliumlike ions beyond $Z \approx 17$, the 2^3P_2 level decays largely by magnetic quadrupole emission. All four of these decays are indicated on the energy-level diagram of Fig. 1. The energies given here are those associated with the transitions in the hydrogenlike ion Ar^{+17} and the heliumlike ion Ar^{+16}.

The lack of experimental information derives from the formidable problems associated with the long lifetimes involved. However, all of these lifetimes decrease very rapidly with increasing Z; hence the recent development of high-energy accelerators of heavy ions, coupled with the beam-foil technique for producing hydrogenlike and heliumlike ions, makes possible tests of the theory under relatively favorable experimental conditions.

In this paper we present the results of a beam-foil experiment designed to study these decays in Ar^{+17} and Ar^{+16} ions obtained at the Berkeley heavy ion linear accelerator (HILAC). Prior publications[2] have already reported the results of some of this work. In this paper, the details are substantially elaborated and a new result for the lifetime of the 2^1S_0 state of Ar^{+16} is given.

I. THEORY

A. Decay of $2^2S_{1/2}$ State of Hydrogenlike Atoms

The possible decay modes of the hydrogen meta-

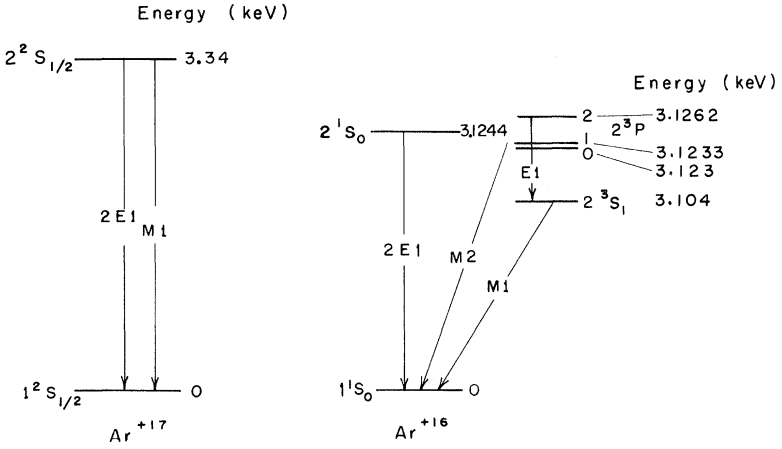

FIG. 1. Energy levels and decay schemes of hydrogenlike Ar^{+17} and heliumlike Ar^{+16}.

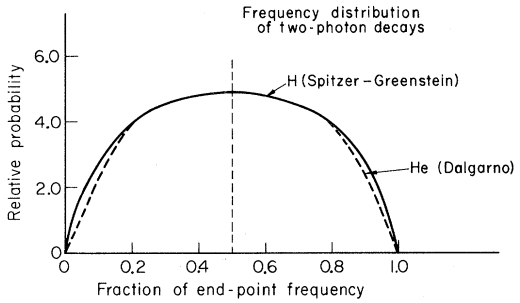

FIG. 2. Predicted nonrelativistic frequency distribution of photons from two-photon decay of the $2\,^2S_{1/2}$ state of Ar^{+17} and the $2\,^1S_0$ state of Ar^{+16}.

stable state were first considered in detail by Breit and Teller.[1] The only single-photon multipole mode to the $1\,^2S_{1/2}$ ground state allowed by the parity and angular momentum selection rules is magnetic dipole ($M1$). However, it is easily seen that, in the nonrelativistic approximation, the transition probability $A_{M1}(2\,^2S_{1/2})$ associated with this decay mode vanishes. One can write

$$A_{M1}(2\,^2S_{1/2}) \propto |\langle 1S|\vec{\mu}|2S\rangle|^2, \tag{1}$$

with $\vec{\mu}$ the magnetic dipole operator, which in nonrelativistic approximation is

$$\vec{\mu} = -\mu_B[\vec{l} + 2\vec{s}] \quad (\mu_B \equiv \text{Bohr magneton}) . \tag{2}$$

It is clear, therefore, that the orthogonality of the radial part of the $1S$-state and $2S$-state eigenfunctions will cause (1) to vanish. Breit and Teller pointed out that, using Dirac theory, there will be a finite value for $A_{M1}(2\,^2S_{1/2})$. This arises because the Hamiltonian responsible for radiative decay is

$$\mathcal{H}_{\text{rad}} = -e\vec{\alpha}\cdot\vec{A} , \tag{3}$$

with $\vec{\alpha}$ the Dirac matrices

$$\vec{\alpha} \equiv \begin{pmatrix} 0 & \vec{\sigma} \\ \vec{\sigma} & 0 \end{pmatrix}$$

and $\vec{A}$ the vector potential of the radiated wave. Using the Hamiltonian (3), Breit and Teller made an estimate of the magnetic dipole rate. However, in their calculation, finite wavelength corrections arising from higher-order terms in the expansion of the plane wave factor $e^{-i\vec{k}\cdot\vec{r}}$ were neglected, and it has recently been pointed out by Drake,[3] Schwartz,[4] and Feinberg and Sucher[5] that these terms make a substantial contribution to the rate. Their calculations show that, for the hydrogenic ions, one obtains for the rate

$$A_{M1}(2\,^2S_{1/2}) = 2.50\times10^{-6}\,Z^{10}\ \text{sec}^{-1}. \tag{4}$$

However, the dominant decay mode of the $2\,^2S_{1/2}$ state of low-Z hydrogenlike ions is not relativistic $M1$ decay but the simultaneous emission of two photons, a process first suggested by Mayer.[6] The two photons have electric dipole ($E1$) character and frequencies ν_1 and ν_2 which satisfy the Bohr condition

$$h(\nu_1 + \nu_2) = \Delta E , \tag{5}$$

where ΔE is the $2S$-$1S$ energy difference.

The frequency distribution of the two photons was first calculated by Spitzer and Greenstein[7] and is plotted in Fig. 2. It is seen to be a broad relatively flat-topped distribution, which, by virtue of Eq. (5), is symmetrical about the midpoint. This distribution is valid for any hydrogenlike ion.

The transition rate $A_{2E1}(2\,^2S_{1/2})$ associated with this mode was first estimated by Breit and Teller, and latter calculated more accurately by Shapiro and Breit[8] and others,[9] with the result

$$A_{2E1}(2\,^2S_{1/2}) = 8.226Z^6\ \text{sec}^{-1} . \tag{6}$$

This rate is based entirely on a nonrelativistic calculation, and there has so far been no calculation using Dirac theory.

It is of some interest to note that, even though the two-photon rate predominates at low Z, $A_{M1} \approx A_{2E1}$ at a value $Z \approx 45$, so that for higher Z the magnetic dipole mode is dominant. In this connection, it should be noted that Boehm and others[10] have recently reported observation of the magnetic dipole transition $2\,^2S_{1/2}$-$1\,^2S_{1/2}$, i.e., the so-called KL_I transition in the x-ray spectra of heavy elements. This would seem to confirm the existence of a crossover point.

Further interest in the lifetime of the $2\,^2S_{1/2}$ state arises from the near degeneracy with the $2\,^2P_{1/2}$ state. The $2\,^2P_{1/2}$ state decays to the ground state via an allowed electric dipole transition with rate[11]

$$A_{E1}(2\,^2P_{1/2}) = 6.25\times10^8\,Z^4\ \text{sec}^{-1} . \tag{7}$$

Consider now the possibility that the $2\,^2S_{1/2}$ wave function is not pure but contains, in fact, a small admixture of the $2\,^2P_{1/2}$ eigenfunction, so that

$$\psi(2\,^2S_{1/2}) = \Phi(2\,^2S_{1/2}) + \epsilon\Phi(2\,^2P_{1/2}) , \tag{8}$$

where ψ is the actual $2\,^2S_{1/2}$-state eigenfunction and the Φ's are the Schrödinger solutions for the hydrogen atom. The decay rate then becomes

$$A(2\,^2S_{1/2}) = A_{M1}(2\,^2S_{1/2}) + A_{2E1}(2\,^2S_{1/2}) + \epsilon^2 A_{E1}(2\,^2P_{1/2}) . \tag{9}$$

Hence, even a very small admixing parameter ϵ can have a dramatic effect on the lifetime and conversely, even a very crude measurement of A can place a very strict limit on ϵ.

Since the parities of the $2S$ and $2P$ states are different, a nonzero value for ϵ implies the presence of an interaction in the atomic Hamiltonian that violates either parity (P) or both parity and

time reversal (PT). The possibility of a P- and T-violating interaction that would manifest itself in the form of a permanent electric dipole moment of the electron (EDM) was considered by Salpeter[12] and Feinberg.[13] Using their formulas, however, the current upper limit[14] to the EDM shows that there can be no effect on the $2\,^2S_{1/2}$ lifetime to less than 1 part in 10^7.

The nonexistence of an EDM does not, however, rule out the possibility of a nonzero value for ϵ arising from a P-violating interaction which does not violate T. Such a mechanism has in fact been considered by Zeldovich and Perelemov,[15] who showed that, if neutral currents are present in the weak interaction, these would give rise to an effect on the $2\,^2S_{1/2}$ lifetime in hydrogen. Conversely, it can be argued that an upper limit on ϵ places a limit on the presence of neutral currents in the weak interaction Hamiltonian.

Another mechanism arises from the possibility that the electromagnetic interaction of a spin-$\frac{1}{2}$ particle contains P-violating terms.[16] The effect of such a term on the $2S$ state of hydrogenic ions has been calculated by Sakitt and Feinberg,[17] and an upper limit on the presence of such a term has been deduced from the available experimental data. As will be seen, the present experiment reduces this limit by greater than a factor of 4.

The two-photon decay of the $2\,^2S_{1/2}$ state was first observed in singly ionized helium by Lipeles, Novick, and Tolk,[18] who reported detection of coincidences and angular distribution measurements consistent with the $1 + \cos^2\theta$ prediction. Spectral measurements in rough agreement with the predicted frequency spectrum were also reported.[19] However, prior to the present work, there have been no lifetime measurements reported.

B. Decay of $2\,^1S_0$ State of Heliumlike Atoms

The metastable $(1s2s)\ 2\,^1S_0$ state can also decay to the ground $(1s)^2\ 1\,^1S_0$ state by a double-photon emission process. However, no single-photon decay mode is possible because of the rigorous selection rule forbidding $0 \nrightarrow 0$ transitions. Hence two-photon decay is necessarily the fastest mode, and the similarity with the hydrogenic two-photon decay is clear when it is noted that the $1s$ electron does not participate in the transition, but acts as a spectator which shields the nuclear charge. The frequency distribution[20] of the photons is very similar to the hydrogenic distribution and is also shown in Fig. 2. Dalgarno and collaborators[21] have done extensive calculations on the decay rate of this state and have obtained the value $A_{2E1}(2\,^1S_0) = 51.8$ sec^{-1} for ordinary helium.[22] An interesting feature of these calculations concerns the asymptotic lifetime in the limit of very high Z. It might be expected that the decay rate $A_{2E1}(2\,^1S_0)$ would approach the hydrogenic rate with a slightly decreased value of Z to take into account shielding by the $1s$ electron. However, it has been noted that[22] in fact the rate approaches roughly twice the hydrogenic rate, the extra factor of 2 coming from the Pauli principle. Thus, for large Z, we can write the rate as

$$A_{2E1}(2\,^1S_0) = 2(8.226)\,(Z-\sigma)^6\ \text{sec}^{-1}\ , \qquad (10)$$

where σ is a shielding constant that must be determined.

Experimentally, there are two previous measurements of the lifetime $\tau(2\,^1S_0)$ in ordinary helium. Pearl[23] and Van Dyck, Johnson, and Shugart[24] have measured the decay in flight of a beam of metastable helium and have obtained, respectively, $\tau(2\,^1S_0) = 38(8)$ msec and $\tau(2\,^1S_0) = 20(2)$ msec. Although the two experimental values are in serious disagreement with each other, the value of Van Dyck *et al.* is in good agreement with theory. In both these experiments the metastable atoms, rather than photons, were detected. In other work a continuous spectrum observed in a neon plasma[25] was attributed to the two-photon decay of the $2\,^1S_0$ state of the heliumlike ion Ne IX.

C. Decay of $2\,^3S_1$ State of Heliumlike Atoms

The decay of the $2\,^3S_1$ state to the $1\,^1S_0$ state had long been thought to proceed primarily by spin-orbit-induced two-photon emission. In this process, first suggested by Breit and Teller,[1] the intermediate P level is an admixture of $^3P_1$ and $^1P_1$ as a result of the spin-orbit coupling, and the two-photon decay rate is nonvanishing. The rates associated with this process have been accurately calculated by Drake, Victor, and Dalgarno[22] and Bely and Faucher.[26] However, there have recently been several reports[27] of the observation in the solar corona of single-photon emission at the wavelength of the $2\,^3S_1$-$1\,^1S_0$ transition in heliumlike ions. The assignment of these lines to this transition was suggested by Gabriel and Jordan,[28] and the emission was ascribed to a relativistically induced magnetic dipole process of the type discussed in connection with the decay of the $2\,^2S_{1/2}$ state of hydrogen. Gabriel and Jordan[29] also emphasized the astrophysical importance of the decay rate of the $2\,^3S_1$ state, showing that measured intensity ratios of the lines $2\,^1P_1 \rightarrow 1\,^1S_0$, $2\,^3P_1 \rightarrow 1\,^1S_0$, and $2\,^3S_1 \rightarrow 1\,^1S_0$ for heliumlike ions could be coupled with this rate to determine the electron density in the solar corona. Subsequently, calculations were made by Schwartz,[4] Drake,[3] and Feinberg and Sucher[5] of the rate associated with this process. In the approach of Schwartz and Drake, the starting point of the calculation is the two-electron Dirac-Breit Hamiltonian, while Feinberg and Sucher start directly from the external-field Hamiltonian of quantum electrodynamics. Both approaches yield identical

results for the effective $M1$ transition operator, which, in the high-Z limit, yields for the decay rate

$$A_{M1}(2^3S_1) = 1.66\times10^{-6}\, Z^{10}\ \text{sec}^{-1}.$$

D. Decay of 2^3P_2 State of Heliumlike Atoms

Magnetic quadrupole ($M2$) radiation is generally of no consequence in atomic physics, since $M2$ rates are of order $(Z\alpha)^4$ slower than $E1$ rates. However, Mizushima[30] first called attention to the possibility that $M2$ radiation might be of astrophysical significance for atomic transitions satisfying the selection rule $\Delta S = \pm 1$. Subsequently Garstang[31] pointed out that the spectrum of heliumlike ions beyond chlorine ($Z = 17$) yields the possibility of observing a magnetic quadrupole transition in the decay 2^3P_2-1^1S_0. At first view, this is an extremely surprising conclusion. In ordinary helium, the 2^3P_2 level decays to the 2^3S_1 level (see Fig. 1) by a fully allowed electric-dipole transition, with a rate[32] $A_{E1}(2^3P_2) = 10^7\ \text{sec}^{-1}$. However, the Z dependence of this rate can be found by noting that

$$A_{E1}(2^3P_2) \propto \omega^3 |\langle 2^3P_2|e\vec{r}|2^3S_1\rangle|^2,$$

where ω is the Bohr frequency for the transition and $\langle|e\vec{r}|\rangle$ is the matrix element of the electric dipole operator. Now for the 2^3P_2-2^3S_1 transition, the Bohr frequency is determined mainly by the electrostatic repulsion of the electrons e^2/r_{12} and since lengths scale as $1/Z$ for large Z, one concludes that $\omega \propto Z$ and $\langle|e\vec{r}|\rangle \propto 1/Z$, so that $A_{E1}(2^3P_2) \propto Z$, for large Z. On the other hand, the $M2$ rate is

$$A_{M2}(2^3P_2) \propto \omega^5 |\langle 2^3P_2|e\vec{r}|1^1S_0\rangle|^2,$$

where now the Bohr frequency is determined by the interaction with the nucleus Ze^2/r, so that $\omega \propto Z^2$ and $A_{M2}(2^3P_2) \propto Z^8$. Hence, it is clear that at some value of Z the $M2$ rate should be dominant. Both Garstang[31] and Drake[33] conclude that, on the basis of numerical calculations, the crossover point occurs around $Z = 17$.

II. EXPERIMENT

A. General Apparatus

These experiments were performed at the Berkeley heavy ion linear accelerator (HILAC) with the 412-MeV argon beam. At this energy, corresponding to a beam velocity $v = 4.4\times10^9$ cm/sec, exponential ($1/e$) decay lengths ($\lambda = v\tau$) are of the order of cm for nsec lifetimes, i.e., relatively convenient for laboratory measurements. The experiments are conveniently done with a beam current of about 10^{-9} A, although the HILAC can deliver substantially more than this.

The apparatus is shown in Fig. 3. Basically, the argon beam from the HILAC is passed through a steering magnet which deflects the beam into a long pipe. The beam is passed through a series

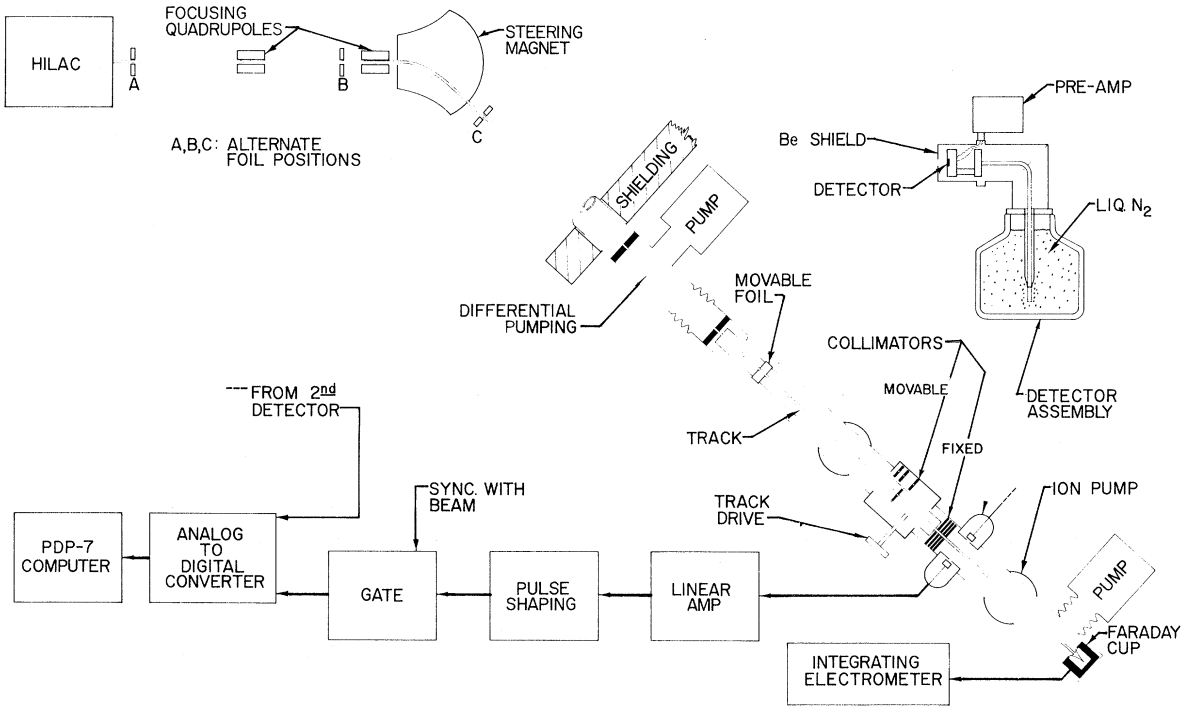

FIG. 3. Schematic diagram of the experimental apparatus.

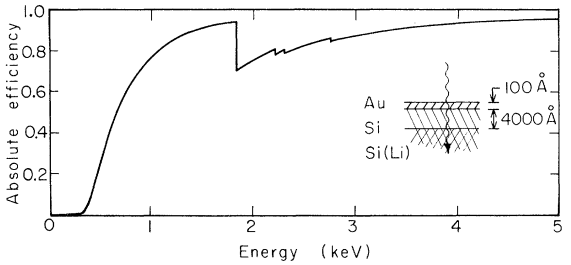

FIG. 4. Computed absolute efficiency of the detectors used in these measurements. The sensitive volume of the detector was assumed to be overlaid with an insensitive Si layer 4000 Å thick.

of collimators and then through a thin foil mounted on a movable track that has a total motion of about 200 cm along the beam. The beam-foil interaction produces ions in the metastable states of interest here and the subsequent decays in flight of atoms in the beam can be observed by a pair of Si (Li) x-ray detectors placed opposite each other and collimated to accept x rays emitted perpendicular to the beam. The beam then impinges on a Faraday cup connected to an integrating electrometer, which measures the total charge collected for normalization purposes. By varying the separation between the foil and the detectors, the decay length can be measured. There is no detectable beam current loss as the foil position is varied.

B. Beam Preparation

For foils beyond a critical thickness, a situation of charge equilibrium exists, and the charge distribution of the emerging beam is roughly independent of such parameters as foil thickness, foil material, and the charge state of the incident beam.[34] The velocity and the atomic number of the incident ion seem to be the dominant parameters. It is found empirically that near-charge equilibrium is obtained for foil thicknesses of $\geq 100\ \mu g/cm^2$. For example, it is found that, with both a 100-$\mu g/cm^2$ Be foil and a 600-$\mu g/cm^2$ Ni foil, the charge distribution that emerges is roughly Ar^{+18} (25%), Ar^{+17} (50%), and Ar^{+16} (25%), and this is roughly independent of the charge state of the incident ions.

For actual lifetime measurement, it is necessary to use beams that are, as much as possible, either pure hydrogenlike or pure heliumlike. To this end, a simple technique for improving on the charge equilibrium situation was found. To enrich the Ar^{+17} content, a "thick" (>100-$\mu g/cm^2$) foil capable of producing charge equilibrium was placed at position A in Fig. 3. The steering magnet was then adjusted to pass only fully stripped (Ar^{+18}) ions into our beam pipe. A "thin" (10-$\mu g/cm^2$) carbon foil was now mounted on our track. Since this foil was much thinner than necessary to reach charge equilibrium, it was expected that single-electron captures (yielding Ar^{+17}) would dominate over double captures (yielding Ar^{+16}). Several independent measurements indicate that $Ar^{+17}/Ar^{+16} \approx 20:1$ using this technique.

Similarly, it was found that, by passing the HILAC beam in the +14 charge state directly through the thin carbon foil, a ratio $Ar^{+16}/Ar^{+17} \gtrsim 6:1$ could be obtained. It is expected that these enrichment ratios can be improved appreciably when more data on charge distributions vs energy, foil thickness and material, and incident charge state become available.

C. Detectors

The detectors used in this experiment are high-resolution Si (Li) x-ray detectors of the type developed by the Lawrence Radiation Laboratory nuclear chemistry electronics group. A schematic of the detector assembly is shown in Fig. 3. Two such detectors were placed on opposite sides of the beam facing each other at distances from 1 to 5 cm from the beam. The detector crystal was 5 mm in diam and 1 mm thick and had a gold layer about 100 Å thick on the front surface. No cover was used over the detector, in order to retain high efficiency at low energies. A 0.01-in.-thick Be plate with a 5-mm-diam hole was supported in front of each detector to prevent detection of extraneous x rays (e.g., from the chamber). The over-all computed efficiency of these detectors is plotted in Fig. 4.

The energy calibration and resolution of the detectors were obtained using x rays from low-intensity radioactive sources. Microcurie amounts of ^{55}Fe and ^{241}Am provided a variety of lines from 5.9 to 22.8 keV. A 1-mC ^{55}Fe source was used to excite by fluorescence x rays of P (~2 keV), Cl (2.6, 2.8 keV), Ca (3.7, 4.0 keV), and Ti (4.5, 4.9 keV), thus bracketing the argon energies near 3 keV. From the pulse-height spectra of these calibration sources, it was determined that, within the resolution of the system, the energy scale is linear and passes through the origin, i.e., the pulse height is a true measure of photon energy. A sample pulse-height vs energy calibration curve is shown in Fig. 5.

D. Data Handling and Analysis

The pulses from the detectors were amplified and shaped using standard high-rate pulse electronics. If single photons were being examined, they were fed directly to the input of an analog-to-digital converter (ADC) which was read by a PDP-7 computer. If coincident photons were being studied, a coincidence circuit was used. This circuit consisted of a pair of pulse differentiators and fast shapers that operated a time-to-amplitude

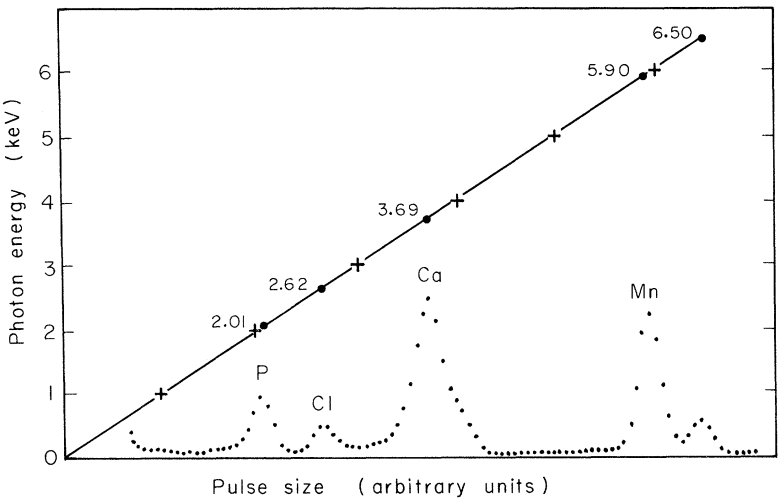

FIG. 5. Typical pulse-height calibration spectrum used to determine the absolute energy scale of the detectors. The energy of each peak is accurately known and allows converting pulse size to energy. The linearity of the scale is clearly in evidence.

converter (TAC), and appropriate gates for the analog signals. If two pulses arrived within a fixed time interval, they were passed on to a multiplexer, which presented the data sequentially to the ADC. In addition, pulses representing the time difference between "coincident" pulses, and the analog sum of the two pulses, could be generated and were fed to the multiplexer as additional data.

The accumulation of spectra could be observed in real time on an oscilloscope screen, which displayed the number of pulses vs pulse size. The accumulation ran continuously under program control, accepting counts whenever they were presented to the ADC. Spectra could be plotted or stored on magnetic tape for later analysis.

The analysis of the spectra was generally performed off line. Standard functions such as energy calibration, peak analysis, integration, and coincidence sorting were used.

III. IDENTIFICATION OF THE DECAY MODES

A. Identification of $2E1$ Decay of $2\,^2S_{1/2}$ State of Ar^{+17}

Identification of the two-photon decay of the $2\,^2S_{1/2}$ level of Ar^{+17} is based mainly on coincidence techniques. A spectrum of the observed decay with the Ar^{+17}-enriched beam and a foil located a few centimeters from the target is shown in Fig. 6. The continuous spectrum is clearly in evidence and is in rough agreement with a broad flat-topped spectrum. Unfortunately, detector efficiency problems and electronic noise prevent measurement of the spectrum below about 500 eV, and single-photon decays distort the spectrum near the end point.

Coincidence detection of the decay photons was done with standard circuitry having a resolving time of about 1 μsec. In the coincidence mode, the detection of two photons in separate detectors within a time interval $|T_1 - T_2| \lesssim 5$ μsec was defined as a "coincidence." For each such event, the computer stores the photon energies E_1 and E_2 registered in the two detectors, the sum energy $E_1 + E_2$ obtained by mixing the amplifier outputs for E_1 and E_2, and the time difference between the pulses $T_1 - T_2$, generated by the TAC. With a typical beam current of 1 nA, coincidence rates were 0.1–1 sec^{-1}.

Figure 7(a) is a plot of the number of events vs the time delay $T_1 - T_2$ between the two photons. The zero in this plot was generated by introducing a fixed delay in one detector; it was calibrated using a pulse generator to simulate a true coincidence. The peak in the time spectrum of Fig. 7(a) is strong evidence that real coincident events were observed.

The energy spectra observed in coincidence mode are shown in Figs. 7(b) and 7(c). These spectra represent only the true coincidences appearing under the peak of the time spectrum in Fig. 7(a).

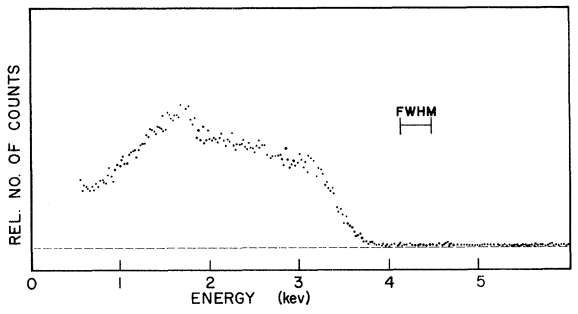

FIG. 6. Typical observed single-photon spectrum identified as the two-photon decay $2\,^2S_{1/2} \rightarrow 1\,^2S_{1/2}$ of Ar^{+17}. These raw data have not been corrected for, e.g., the efficiency plotted in Fig. 4.

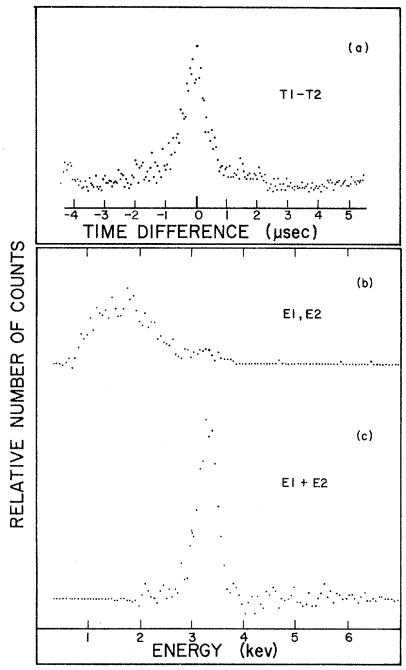

FIG. 7. Typical observed spectra of Ar^{+17} using coincidence mode. (a) Number of events vs time delay between photons; (b) number of photons contributing to a coincident event vs energy; (c) number of events vs sum energy of two photons.

The contribution to that peak by accidental coincidences was removed by subtracting an equivalent number of events occurring away from the peak (presumably all accidentals), suitably normalized. The main difference between the singles spectra in Figs. 6 and 7(b) is that the coincidence spectra are roughly the square of the singles spectra, thereby symmetrically discriminating against the ends of the continuum, peaking it more strongly at the center. The spectrum associated with the sum energy E_1+E_2 observed as true coincidences is shown in Fig. 7(c). Except for residual noise

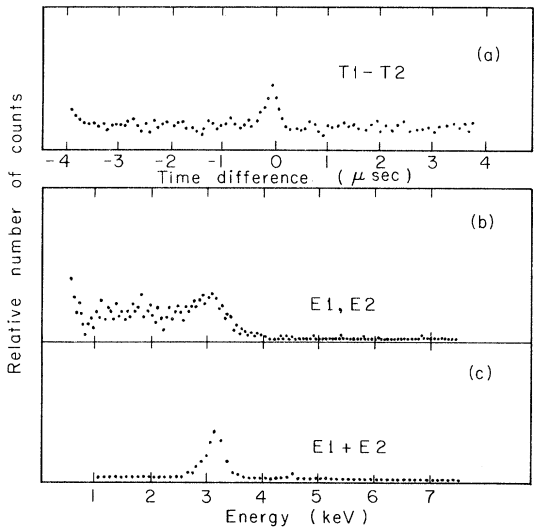

FIG. 9. Typical observed spectra of Ar^{+16} using coincidence mode. (a) Number of events vs time delay between photons; (b) number of photons contributing to a coincident event vs energy; (c) number of events vs sum energy of two photons.

due to accidentals that have been removed, the spectrum is a single strong peak with a width roughly equal to the system resolution, which indicates that this peak represents a single line. That this line falls at 3.3 keV is also strong evidence of the two-photon mode in Ar^{+17} and not Ar^{+16}, since the latter would give a peak at 3.1 keV.

B. Identification of $2E1$ Decay of the $2\,^1S_0$ State of Ar^{+16}

The singles spectrum obtained with the enriched Ar^{+16} is shown in Fig. 8. The continuous spectrum characteristic of two-photon emission is again in evidence. A coincidence spectrum taken with this

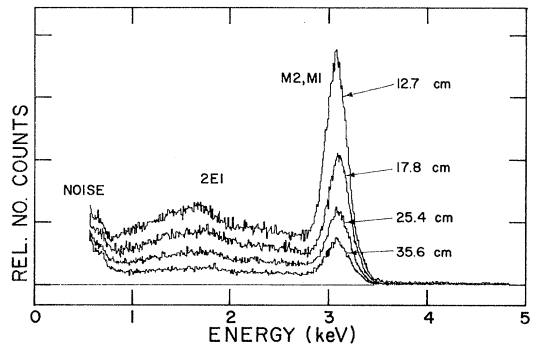

FIG. 8. Typical observed single-photon spectra of Ar^{+16}, for several foil-detector distances.

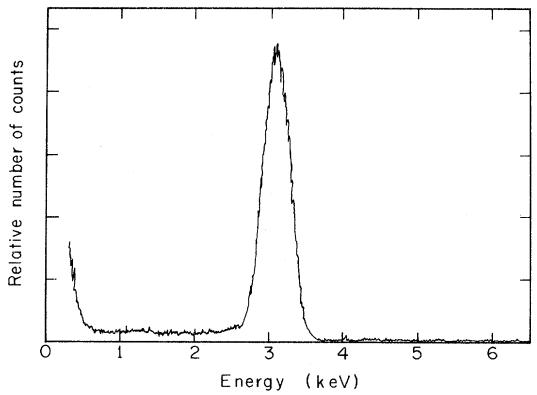

FIG. 10. Typical observed spectrum identified as the relativistically induced magnetic dipole transition $2\,^3S_1 \rightarrow 1\,^1S_0$ of Ar^{+16}.

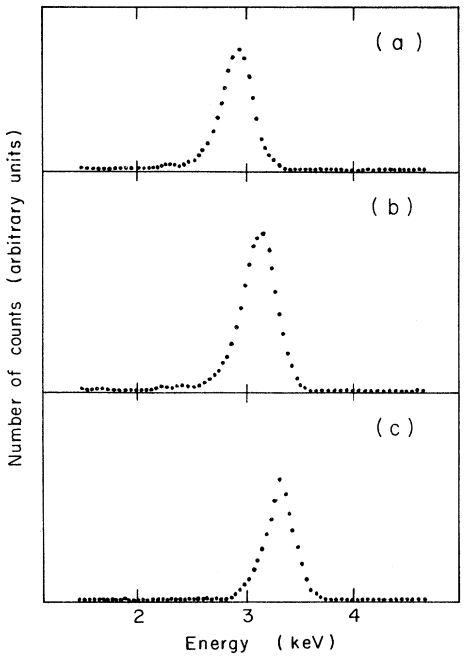

FIG. 11. Doppler shift of the $M1$ line of Fig. 10. (a) Detector viewing downstream; (b) detector viewing perpendicular to beam; (c) detector viewing upstream.

beam is shown in Fig. 9.

Unfortunately, these data are not of sufficient quality to distinguish this spectrum from that associated with two-photon decay of Ar^{+17}, although the intensity and the fact that it is obtained with the Ar^{+16}-enriched beam is suggestive. However, a decay curve taken with this spectrum (Fig. 14) shows that it decays with a lifetime that is substantially faster than the lifetime associated with the Ar^{+17} beam, and is also in good agreement with the theoretical lifetime for the decay of the $2\,^1S_0$ state of Ar^{+17} (see Sec. IV B).

C. Identification of $M1$ Decay of $2\,^3S_1$ State of Ar^{+16}

In order to identify the $M1$ decay mode of the $2\,^3S_1$ level of Ar^{+16}, advantage can be taken of the extremely long decay length (~ 8 m) associated with this mode. Hence a foil placed several meters upstream of the detectors will be sufficiently far away that all levels except $2\,^3S_1$ will have decayed to the ground level by the time the ions are in the field of view of the detectors. A spectrum taken with the foil 6 m from the detectors is shown in Fig. 10. The single peak at 3.1 keV is somewhat Doppler broadened, but is at the correct energy[35] for the $2\,^3S_1$-$1\,^1S_0$ decay. To establish that the observed x ray arises from a decay in flight of a beam ion, an adjustable slit was mounted in front of the detector. The slit position determines whether the detector views upstream, downstream, or straight ahead, and therefore permits observation of the Doppler shift. The spectra obtained with the slit in the three viewing positions are shown in Fig. 11. The Doppler shift is clearly visible and is roughly consistent with the expected shift.

TABLE I. Observed and predicted energies ($2\,^3S_1$-$1\,^1S_0$) in keV.

	Si XIII	S XV	Ar XVII
Observed	1.85 (0.10)	2.46 (0.10)	3.13 (0.10)
Predicted (Ref. 35)	1.84	2.42	3.09

To corroborate that the decay arises from an ion in the beam, spectra were obtained with beams of sulphur ($Z = 16$) and silicon ($Z = 14$) and are shown in Fig. 12. Because of the longer lifetimes involved, the two-photon continua begin to appear. A comparison of measured energies with theoretical energies is shown in Table I. On the basis of this agreement and the long lifetimes involved, we conclude that the observed decay is indeed the single-photon $2\,^3S_1$-$1\,^1S_0$ transition.

D. Identification of $M2$ Decay of $2\,^3P_2$ State of Ar^{+16}

As indicated in Fig. 1, the energy associated with the transition $2\,^3P_2$-$1\,^1S_0$ differs from the $2\,^3S_2$-$1\,^1S_0$ transition energy by only 22 eV. The emission lines are not resolved by our detectors, which have a width of about 200 eV. That the observed line at 3.12 keV (Fig. 6) actually consists of two components is established by the decay curve of Fig. 17. The slow decay is associated with the decay of the $2\,^3S_1$ state, whereas the lifetime associated with the fast decay is in good agreement with the theoretical lifetime of the $2\,^3P_2$ state (see Sec. IV D).

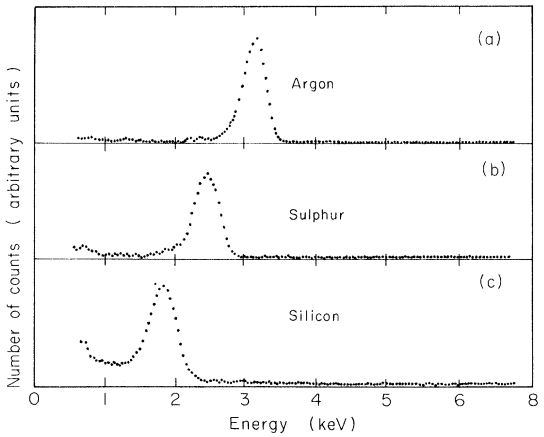

FIG. 12. Z dependence of the $M1$ line of Fig. 10. (a) Argon, $Z = 18$; (b) sulphur, $Z = 16$; (c) silicon, $Z = 14$.

IV. LIFETIME DATA

The lifetimes are measured by plotting the intensity of the emission spectra ($2E1$, $M1$, $M2$) as a function of foil-detector separation. As a measure of this intensity, we used the total counts registered in an appropriate energy interval. The total number of counts is normalized to the total integrated beam current measured with the Faraday cup. Since the decay of the state is exponential in time, the count rate is exponential in distance, so a least-squares fit to the function

$$N(x) = N(0)e^{-x/v\tau}$$

can be made, thus determining τ.

A. Decay of $2^2S_{1/2}$ State of Ar^{+17}

The beam used for this measurement is the enriched Ar^{+17} prepared by the two-foil technique described in Sec. IIB. The singles spectrum obtained with this beam is shown in Fig. 6. There are two facts which lead us to believe that the spectrum is almost entirely due to real counts associated with two-photon decay from the $2^2S_{1/2}$ state. First we note from Fig. 7 that this spectrum is in reasonable agreement with the singles spectrum obtained only from coincident events. There is, however, a rise on the high-energy end, which is due to decays from the $M1$ transition of the helium-like ions. Secondly, the coincident sum energy $E_1 + E_2$ falls at 3.3 keV, the energy of the transition in Ar^{+17}.

Furthermore, the background rate at energies greater then 3.3 keV is only about 1% of the mean rate at energies less than 3.3 keV. Hence it was concluded that it was not necessary to use coincident events for the lifetime measurement. Since the singles rate is about 1000 times more rapid than the rate for coincident events, an accurate value can be obtained correspondingly faster.

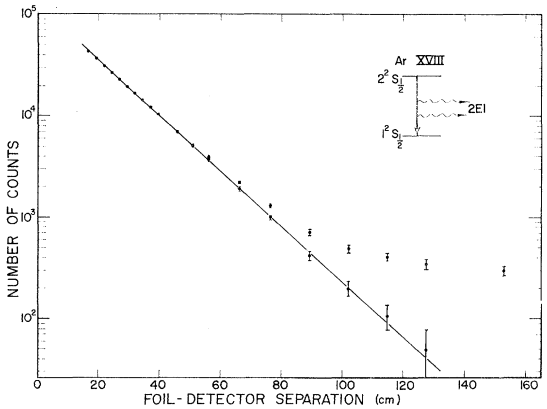

FIG. 13. Typical decay curve of the $2E1$ spectrum of Ar^{+17} shown in Fig. 6.

TABLE II. Summary of measurements of $\tau(2^2S_{1/2})$.

τ (nsec)[a]	σ (nsec)[b]	Weight[c]
3.46	0.15	0.4
3.63	0.10	0.5
3.60	0.10	0.5
3.62	0.10	1.0

[a]Uncorrected raw data.
[b]Represents 67% confidence.
[c]Assigned according to general quality and reliability of data.

The normalized count rate was obtained by integrating the continuous spectrum in Fig. 6 between various limits. Normally the low-energy cutoff was chosen to avoid counts due to electronic noise, while the high-frequency cutoff was chosen to avoid counts from $M1$ and $M2$ decays of any metastable Ar^{+16} atoms present in the beam.

Counts were obtained simultaneously in both detectors and the normalized rates averaged. Typical data from one 16-h run are plotted in Fig. 13. It is seen that at large distances the count rate flattens out to a relatively constant background; the origin of this background is not known, but a plausible hypothesis is that it arises from magnetic dipole x rays that are incompletely converted in the x-ray detector. In any case they are a small fraction of the decay rate at small distances, so that the method of treating them does not seem to us to be crucial. In fact, the background is treated as a constant and subtracted from all points on the curve to yield the line shown in Fig. 13. The resultant line appears to be a single exponential over about seven mean ($1/e$) decay lengths, which thus lends support to this subtraction procedure. The decay rate $A(2^2S_{1/2})$ is obtained by dividing the known beam velocity by the mean decay length determined from the plot. The mean lifetime of the state is then $\tau = 1/A$.

The results of several such independent determinations are listed in Table II. To each value, a weighting factor w_i is assigned that indicates the relative quality of the data. The weighted average of the lifetimes $\tau = \sum_i w_i \tau_i / \sum_i w_i$ and the weighted rms deviation $\sigma^2 = \sum_i w_i (\tau - \tau_i)^2 / \sum_i w_i$ is taken as the measured lifetime and its error, respectively. The final result is

$$\tau(2^2S_{1/2}) = 3.54 \pm 0.25 \text{ nsec},$$

where the error is based mainly upon our assessment of the size of possible systematic uncertainties. This value includes a 1% correction for the transverse Doppler effect. The correction for the degrading of the beam energy passing through the carbon foil is negligible.

The possibility of quenching arising from colli-

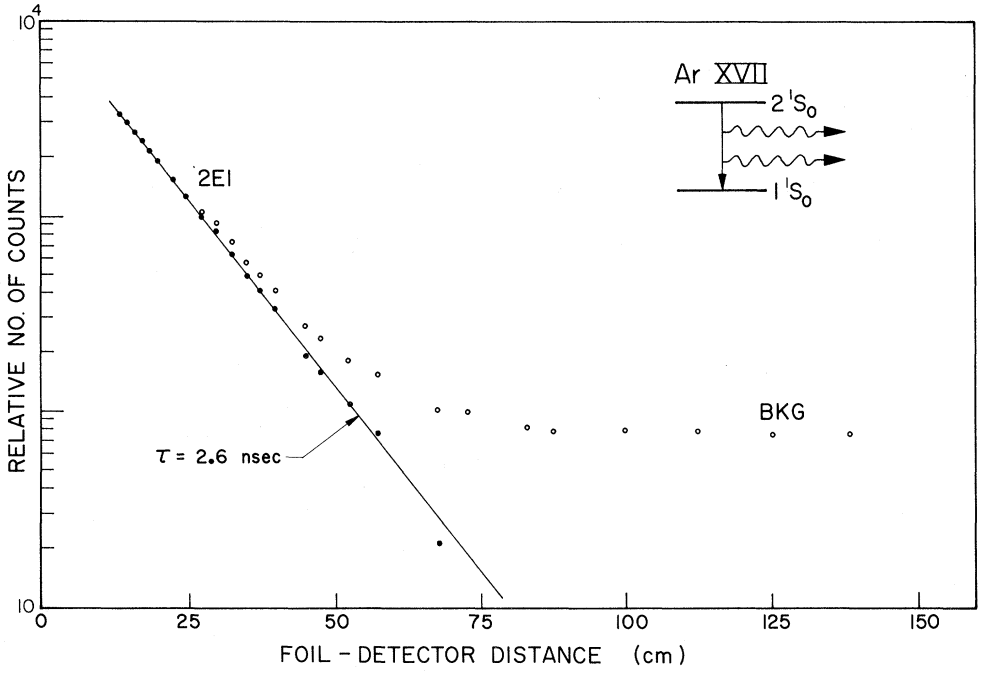

FIG. 14. Typical decay curve of the $2E1$ spectrum of Ar^{+16} shown in Fig. 8.

sion of beam ions with the background gas was studied by increasing the background gas pressure by a factor of 10. No observable effect on the decay rate was measured to within 5%.

B. Decay of $2\,^1S_0$ State of Ar^{+16}

The beam used for this work was the Ar^{+16}-enriched beam described in Sec. IIB. The measurement of the decay rate proceeded in a manner essentially identical to that of the $2\,^2S_{1/2}$ measurement. The interval over which integration was used was somewhat less than in the case of the $2\,^2S_{1/2}$ decay, because of the presence of the strong 3-keV peak. The normalized count rate is plotted against foil-detector separation in Fig. 14. Here again a constant background manifests itself at large separations and the actual decay curve is obtained by subtracting this background from all the points. Table III lists the results of independent determinations of $\tau(2\,^1S_0)$. As before, weights were assigned according to the quality of the data, and the weighted

TABLE III. Summary of measurements of $\tau(2\,^1S_0)$.

τ (nsec)[a]	τ_{corr} (nsec)[b]	σ (nsec)[c]	Weight[d]
2.69	2.48	0.15	0.4
2.53	2.26	0.3	0.1
2.62	2.34	0.2	1.0
2.69	2.34	0.2	1.0
2.63	2.26	0.2	1.0

[a]Uncorrected raw data.
[b]Corrected for admixture of $2\,^2S_{1/2}$ $2E1$ decay.
[c]Represents 67% confidence.
[d]Assigned according to general quality and reliability of data.

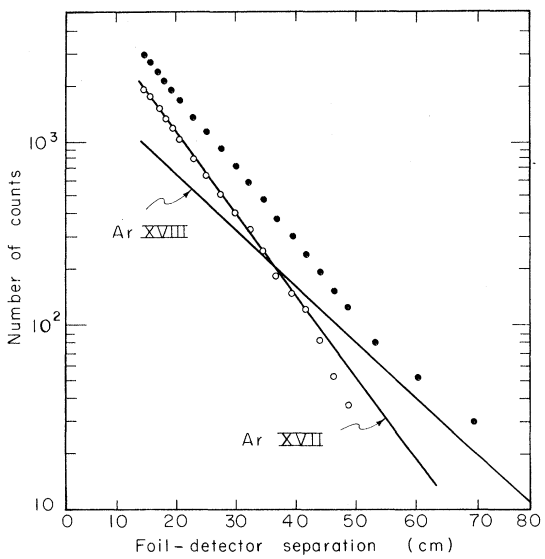

FIG. 15. Typical decay curve of the $2E1$ spectrum of Ar^{+16}, showing correction of the data for the Ar^{+17} $2E1$ decay. The solid circles are the experimental data, the light line is the computed contribution of Ar^{+17}, the open circles are the difference (representing a pure Ar^{+16} decay), and the heavy line is a least-squares fit to the open circles.

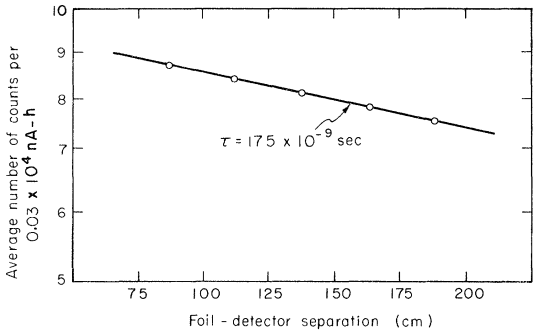

FIG. 16. Typical decay curve of the $M1$ line of Ar^{+16} shown in Fig. 10.

average is quoted as the measured result.

The largest uncertainty associated with this rate arises from contamination of the continuous spectrum by decays associated with the $2\,^2S_{1/2}$ state of Ar^{+17}. Since this spectrum overlaps the region of integration, the presence of such decays will give rise to a bias which would tend to destroy the single exponential character of the decay and to make the "effective" decay length of the observed decay somewhat longer than the true value.

A model for estimating the fraction of $2\,^2S_{1/2}$ decays present can be constructed in the following way. Measurements of the charge distribution show that $N(+17)/N(+16) \approx \frac{4}{27}$. Moreover, on theoretical grounds one can expect that $A(2\,^2S_{1/2}) \approx \frac{2}{3} \times A(2\,^1S_0)$. The problem of estimating the probability per ion of forming the $2\,^1S_0$ and $2\,^2S_{1/2}$ metastable states $P(2\,^1S_0)$ and $P(2\,^2S_{1/2})$, respectively, now remains. A reasonable assumption is that the passive $1s$ electron acts mainly to shield the nucleus, and the levels of the same principal quantum number are identically excited in the Ar^{+16} and Ar^{+17} systems. However, in the case of Ar^{+16}, the electron occupies the triplet state 75% of the time, so we obtain $P(2\,^1S_0) = \frac{1}{4}P(2\,^2S_{1/2})$. With this assumption we conclude that approximately 30% of the decays at the foil belong to Ar^{+17}.

We have used this model to correct the raw data, and a typical decay curve and the subtraction procedure used to obtain the decay rate are shown in Fig. 15. The result obtained in this way is $\tau(2\,^1S_0) = 2.33 \pm 0.1$ sec. The uncertainty in this correction is clearly the largest source of error in our result. However, the measured lifetime seems not to be extremely sensitive to this correction. If a lifetime value is obtained from the uncorrected data, the result is about 15% larger than the value with the correction. Based on our analysis we quote, for the final result,

$$\tau(2\,^1S_0) = 2.3 \pm 0.3 \text{ nsec},$$

where the uncertainty is again based on our estimate of the size of possible systematic errors.

C. Decay of $2\,^3S_1$ State of Ar^{+16}

The mean length associated with the $M1$ decay of the $2\,^3S_1$ state of Ar^{+16} is about 8 m and is substantially longer than the length associated with the decay of any other level. Hence, by looking at distances that are far from the foil, interference from other decay modes can be eliminated. Because of space limitations, the foil was moved only through a total distance of about 1 m, or only about $\frac{1}{8}$ of a mean length, so that the total observable decay is small. The data were accumulated in short time intervals (~ 3 min), moving the foil cyclically through five or six positions in order to average out slow variations in the beam or apparatus or both. A sample decay curve taken with the foil at large distances from the detector is shown in Fig. 16. In Table IV the results of independent measurements of $\tau(2\,^3S_1)$ are summarized. The weighted average and rms deviation were computed as before. The final result including a 1% correction for relativistic time dilation is

$$\tau(2\,^3S_1) = 172 \pm 30 \text{ nsec}.$$

The uncertainty again reflects our estimate of the possible sources of systematic error.

D. Decay of $2\,^3P_2$ State of Ar^{+16}

A plot of the decay of the 3.1-keV line is shown in Fig. 17. As mentioned in Sec. IID, the energy of the $2\,^3P_2$-$1\,^1S_0$ decay cannot be resolved from the $2\,^3S_1$-$1\,^1S_0$, and the observed compound decay is consistent with this fact. If it is assumed that no other decays are present, the separation of this

TABLE IV. Summary of measurements of $\tau(2\,^3S_1)$.

τ (nsec)[a]	σ (nsec)[b]	Weight[c]
162	30	0.1
128	30	0.1
199	40	0.5
175	20	1.0
170[d]	30[d]	0.5[d]
172[d]	15[d]	1.0[d]
159	15	0.4
190	15	0.5
154	15	0.3
172	12	1.0
172	15	0.2
169	12	0.7
200[e]	50[e]	0.1[e]

[a]Uncorrected raw data.
[b]Represents 67% confidence.
[c]Assigned according to general quality and reliability of data.
[d]Pressure 2.5 times normal.
[e]Two foils separated by 16 ft. Nearer foil about 20 ft from detectors.

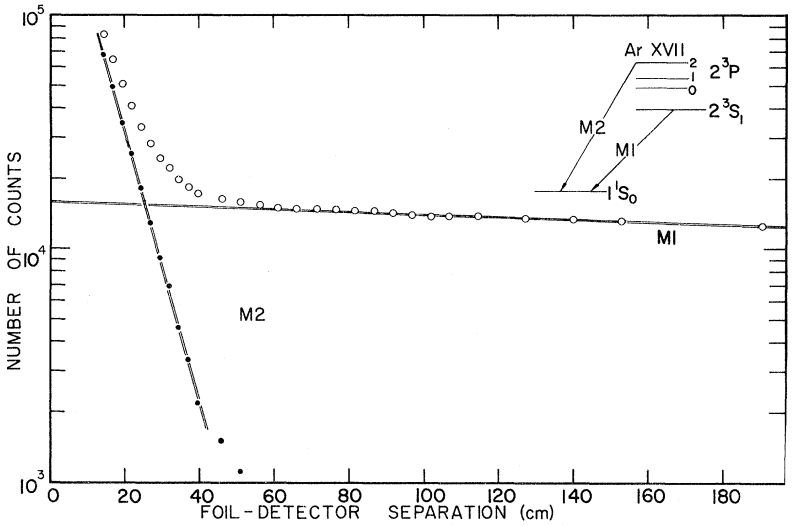

FIG. 17. Typical decay curve of the 3.1-keV line of Ar^{+16} shown in Fig. 8.

curve into two exponential components should be reliable. The lines in Fig. 17 represent this separation, and the slopes yield $\tau(2\,^3P_2)$ and $\tau(2\,^3S_1)$.

In Table V the values of $\tau(2\,^3P_2)$ obtained from independent decay curves are listed. The weighted average result is

$$\tau(2\,^3P_2) = 1.7 \pm 0.3 \text{ nsec},$$

where the error is based on our estimate of the size of possible systematic uncertainties.

V. COMPARISON WITH THEORY

In Table VI a comparison of the measured and theoretical lifetimes is given. Agreement of the measured two-photon rates with the theoretically expected rates is good for both the $2\,^2S_{1/2}$ state and the $2\,^1S_0$ state. However, it should be emphasized that the theoretical values are in both cases based on nonrelativistic calculations. One can argue on rather general grounds that the relativistic corrections to the nonrelativistic rate should be of order $(Z\alpha)^2$, which for argon ($Z=18$) is about 2%. However, this is of the same order as our uncertainty, and hence a relativistic calculation is needed to assure that the agreement is real. Experimentally, we are currently attempting refined measurements that will yield the transition rate to an accuracy of 1% in elements of somewhat higher Z.

If the theoretical and experimental rates are assumed to be in agreement, it then becomes possible to use our result to place an upper limit on a possible parity-violating component of the $2\,^2S_{1/2}$ wave function of Ar^{+17}. The existence of such a parity-violating component has been considered by several authors[12,13] and was discussed in Sec. IA. Let us write $\psi(2\,^2S_{1/2}) = \Phi(2\,^2S_{1/2}) + \epsilon\Phi(2\,^2P_{1/2})$,

TABLE V. Summary of measurements of $\tau(2\,^3P_2)$.

τ (nsec)[a]	σ (nsec)[b]	Weight[c]
1.7	0.15	1.0
1.8	0.2	0.5

[a]Uncorrected raw data.
[b]Represents 67% confidence.
[c]Assigned according to general quality and reliability of data.

TABLE VI. Measured and theoretical lifetimes.

Ion	State	τ_{expt} (nsec)	τ_{theor} (nsec)
Ar^{+17}	$2\,^2S_{1/2}$	3.54 ± 0.25[a]	3.46[b]
Ar^{+16}	$2\,^1S_0$	2.3 ± 0.3[c]	2.35[d]
	$2\,^3S_1$	172 ± 30[a]	210[e]
	$2\,^3P_2$	1.7 ± 0.3[f]	1.49[g]
S^{+15}	$2\,^2S_{1/2}$	7.3 ± 0.7[h]	7.11[b]

[a]Includes 1% correction for relativistic time dilation.
[b]Includes nonrelativistic two-photon decay [Eq. (6)] and relativistic magnetic dipole decay [Eq. (4)].
[c]Includes correction for presence of Ar^{+17} ions (see Sec. IV B); assumes $\tau(2\,^2S_{1/2})$ known.
[d]Nonrelativistic asymptotic (to large Z) value including partial screening by 1s electron [Eq. (10)]. Assumes screening constant $\sigma = 0.797$, which is a variational result of Drake (Ref. 36) for $Z = 10$.
[e]Average of two results: Drake (Ref. 3) (212.7) and Schwartz (Ref. 4) (208). Calculations include leading relativistic and finite wavelength corrections. Asymptotic formula [Eq. (11)] yields 168.7.
[f]Assumes $2\,^3S_1 \rightarrow 1\,^1S_0$ $M1$ decay rate known, so compound decay curve could be analyzed into two simple decays (Sec. IV D).
[g]Assumes calculated value for the $2\,^3P_2 \rightarrow 2\,^3S_1$ $E1$ rate (Sec. V).
[h]Includes correction for presence of S^{+14} (see Appendix); assumes $\tau(2\,^1S_0)$ to be the value calculated from Eq. (10).

where $\psi(2^2S_{1/2})$ is the actual wave function and the Φ's are the solution to the Schrödinger equation for the $2^2S_{1/2}$ and $2^2P_{1/2}$ states, respectively, with ϵ a small numerical parameter we obtain from our experimental uncertainty:

$$|\epsilon| \leq 6\times10^{-4} .$$

Our experiment cannot determine a possible phase factor associated with ϵ.

From our value of ϵ a new upper limit on the magnitude of an electronic pseudocharge (anapole) can be established. In terms of the notation of Sakitt and Feinberg, we obtain

$$\lambda \leq 7\times10^{-5} .$$

This is smaller by more than a factor of 4 than the previous upper limit based on the $2S_{1/2}$ lifetime of He^+.[17] This limit on λ is based on the assumption that the Lamb shift (Δ_L) in the $n=2$ state is given by $\Delta_L = 10^3 Z^4$ MHz. The actual value is as yet uncalculated and may differ substantially from this result.

Our result for the lifetime of the 2^3S_1 level differs somewhat from the theoretical rate. Several possible sources of systematic error were studied. Quenching due to collisions with background gas was studied by varying the pressure over a factor of 3 with no measurable effect. In addition, the independence of the lifetime with respect to foil material and thickness was also established. Perhaps the weakest aspect of this measurement is that it is made over a small fraction of a decay length, and hence the exponential character of the observed decay is not completely established. However, it is important to point out that, if the observed decay is actually a compound decay resulting from "feeding" via decay from higher levels, then the effective lifetime, i.e., the one which is measured, must be longer than the true lifetime. Further experiments are planned on higher-Z ions in order to observe $M1$ decay over several decay lengths.

The decay of the 2^3P_2 level of Ar^{+16} proceeds by two principal mechanisms: $E1$ decay to the 2^3S_1 level and $M2$ decay to the ground 1^1S_0 level. Recently, Drake[36] has computed the $E1$ rate with the result $A_{E1}(2^3P_2) = 3.55\times10^8$ sec^{-1}. If we write

$$1/\tau(2^3P_2) = A_{E1} + A_{M2}$$

and use the value[31,33] $A_{M2}(2^3P_2) = 3.14\times10^8$ sec^{-1}, the theoretically predicted lifetime is $\tau = 1.49\times10^{-9}$ sec, which is within our experimental error.

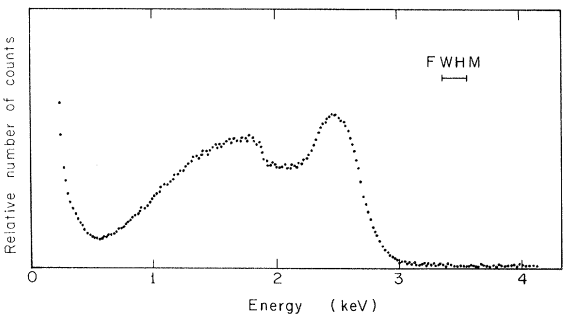

FIG. 18. Observed single-photon spectrum identified as the $2E1$ decay of the $2^2S_{1/2}$ state of S^{+15}.

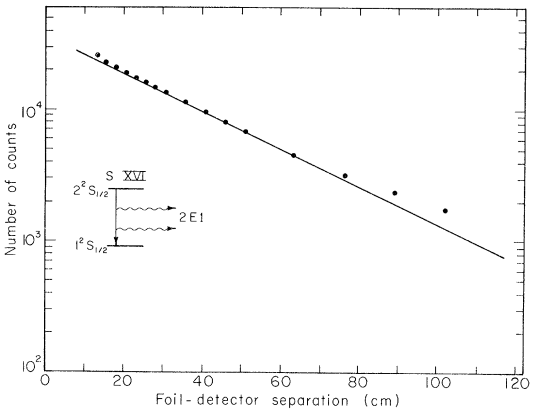

FIG. 19. Observed decay curve of the $2E1$ spectrum of S^{+15} shown in Fig. 18.

ACKNOWLEDGMENTS

Many people have contributed to the success of these experiments. We thank A. Ghiorso for providing time on the HILAC and for his encouragement of this experiment. The nuclear chemistry electronics group of Fred Goulding provided the detectors used in this experiment and provided maintenance and servicing. We thank particularly E. Lampo, D. Malone, R. Pehl, J. Walton, and J. Jaklevic for their unstinting aid. R. Diamond and F. Stephens provided the computer. D. MacDonald and W. Harnden gave engineering assistance and W. Davis helped with the data taking.

APPENDIX: LIFETIME OF $2^2S_{1/2}$ STATE OF HYDROGENLIKE SULPHUR

We have also measured the lifetime of the $2^2S_{1/2}$ state of hydrogenlike sulphur ($Z=16$) using the same techniques described in Secs. II and III A. The singles spectrum observed with the sulphur beam is shown in Fig. 18. This spectrum exhibits the same features seen in the argon spectra: the $M1/M2$ peak at the $2S$-$1S$ energy separation (~ 2.45 keV), the detector Si K absorption edge at 1.84 keV, and the broad continuum between $E=0$ and $E \approx 2.4$ keV identified as the two-photon spectrum. This spectrum was observed on several occasions, but only one decay curve (Fig. 19) was obtained. The lifetime obtained from this decay curve is $\tau(2^2S_{1/2}) = 6.9 \pm 0.5$ nsec. The largest uncertainty

in this result is the contribution of heliumlike ions to the $2E1$ spectrum. We can use the same type of analysis as Sec. IV B to estimate the $2\,^1S_0$-$1\,^1S_0$ S^{+14} contribution. Measurements of the charge distribution gave $N(+14)/N(+15) \approx \frac{1}{4}$. Assuming as before that $A(2\,^2S_{1/2}) \approx \frac{2}{3} A(2\,^1S_0)$ and $P(2\,^1S_0) = \frac{1}{4} \times P(2\,^2S_{1/2})$, we find that, at the foil, $\frac{3}{16}$ of the decays are due to S^{+14} and the rest to S^{+15}. Thus, we can correct the decay curve in the manner of Fig. 15. The final result is

$$\tau(2\,^2S_{1/2}) = 7.3 \pm 0.7 \text{ nsec.}$$

This result can be compared with the nonrelativistic asymptotic prediction [Eq. (6)], $\tau = 7.23$ nsec. The good agreement between theory and experiment tends to confirm our identification of the two-photon decay mode, and the predicted Z dependence of the lifetime. To the extent that, in the two independent cases Ar^{+16} $2\,^1S_0 \rightarrow 1\,^1S_0$ and S^{+15} $2\,^2S_{1/2} \rightarrow 1\,^2S_{1/2}$), the corrections for contaminations from other decays tended to improve the agreement between theory and experiment, our "reasonable" model of the excited-state populations, $P(2\,^1S_0) = \frac{1}{4} \times P(2\,^2S_{1/2})$, is confirmed. In other words, the idea that, so far as one-electron transitions are concerned, a heavy heliumlike ion of atomic number Z acts like a hydrogenlike atom of atomic number $Z - \sigma$ ($\sigma \approx 1$), appears to be supported by our data.

*Work supported in part by U. S. Atomic Energy Commission.

[1]G. Breit and E. Teller, Astrophys. J. 91, 215 (1940).

[2]R. Marrus and R. W. Schmieder, Phys. Letters 32A, 431 (1970); R. W. Schmieder and R. Marrus, Phys. Rev. Letters 25, 1245 (1970); R. Marrus and R. W. Schmieder, *ibid.* 25, 1689 (1970); R. W. Schmieder and R. Marrus, *ibid.* 25, 1692 (1970).

[3]G. W. F. Drake, Phys. Rev. A 3, 908 (1971).

[4]C. Schwartz (private communication).

[5]G. Feinberg and J. Sucher, Phys. Rev. Letters 26, 681 (1971).

[6]M. Goeppert-Mayer, Ann. Physik 9, 273 (1931).

[7]L. Spitzer and J. L. Greenstein, Astrophys. J. 114, 407 (1951).

[8]J. Shapiro and G. Breit, Phys. Rev. 113, 179 (1959).

[9]B. A. Zon and L. P. Rapoport, Zh. Eksperim. i Teor. Fiz. Pis'ma v Redaktsiyu 7, 70 (1968) [Sov. Phys. JETP Letters 7, 52 (1968)]; S. Klarsfeld, Phys. Letters 30A, 382 (1969).

[10]F. Boehm, Phys. Letters 33A, 417 (1970), and references therein.

[11]Evaluated by H. Bethe and E. E. Salpeter, in *Handbuch der Physik* (Springer, Berlin, 1957), Vol. XXXV, p. 352.

[12]E. E. Salpeter, Phys. Rev. 112, 1642 (1958).

[13]G. Feinberg, Phys. Rev. 112, 1637 (1958).

[14]M. C. Weiskopff *et al.*, Phys. Rev. Letters 21, 1645 (1968).

[15]Ya. B. Zel'dovich and A. M. Perelomov, Zh. Eksperim. i Teor. Fiz. 39, 1115 (1960) [Sov. Phys. JETP 12, 777 (1961)].

[16]R. A. Carhart, Phys. Rev. 132, 2337 (1963); J. Bernstein, M. Ruderman, and G. Feinberg, *ibid.* 132, 1227 (1963).

[17]B. Sakitt and G. Feinberg, Phys. Rev. 151, 1341 (1966).

[18]M. Lipeles, R. Novick, and N. Tolk, Phys. Rev. Letters 15, 690 (1965).

[19]C. J. Artura, N. Tolk, and R. Novick, Astrophys. J. 157, L181 (1969).

[20]A. Dalgarno, Proc. Phys. Soc. (London) 87, 371 (1966).

[21]G. A. Victor and A. Dalgarno, Phys. Rev. Letters 25, 1105 (1967), references are given herein to earlier work.

[22]G. W. F. Drake, G. A. Victor, and A. Dalgarno, Phys. Rev. 180, 25 (1969).

[23]A. S. Pearl, Phys. Rev. Letters 24, 703 (1970).

[24]R. S. Van Dyck, Jr., C. E. Johnson, and H. A. Shugart, Phys. Rev. Letters 25, 1403 (1970).

[25]R. C. Elton, L. J. Palumbo, and H. R. Griem, Phys. Rev. Letters 20, 783 (1968).

[26]O. Bely and P. Faucher, Astron. Astrophys. 1, 37 (1969).

[27]W. M. Neupert and M. Swartz, Astrophys. J. 160, L189 (1970); G. A. Doschek, J. F. Meekins, R. W. Kreplin, T. A. Chubb, and H. Friedman, *ibid.* 164, 165 (1971); A. B. C. Walker, Jr. and H. R. Rugge, Astron. Astrophys. 5, 4 (1970), and references therein.

[28]A. H. Gabriel and C. Jordan, Nature 221, 947 (1969).

[29]A. H. Gabriel and C. Jordan, Monthly Notices Roy. Astron. Soc. 145, 241 (1969).

[30]M. Mizushima, Phys. Rev. 134, A883 (1964).

[31]R. H. Garstang, Publ. Astron. Soc. Pac. 81, 488 (1969).

[32]D. A. Landman, Bull. Am. Phys. Soc. 12, 94 (1967).

[33]G. W. F. Drake, Astrophys. J. 158, 119 (1969).

[34]For a review of all aspects of the beam-foil method, see *Beam-Foil Spectroscopy*, edited by S. Bashkin (Gordon and Breach, New York, 1968), Vols. I and II. See also H. H. Heckman, E. L. Hubbard, and W. G. Simon, Phys. Rev. 129, 1240 (1963).

[35]H. T. Doyle, *Advances in Atomic and Molecular Physics* (Academic, New York, 1969), p. 337.

[36]G. W. F. Drake (private communication).